Solid-Phase Thermodynamic Interpretation of Ion Desorption in Matrix-Assisted Laser Desorption/Ionization

Yin-Hung Lai,[†,‡,§] Chia-Chen Wang,[†] Sheng-Hsian Lin,[‡,||] Yuan Tseh Lee,[†] and Yi-Sheng Wang*[,†]

Genomics Research Center, Academia Sinica, Taipei 115, Taiwan, Molecular Science and Technology Program, Taiwan International Graduate Program, Academia Sinica, Taipei 115, Taiwan, Department of Chemistry, National Tsing Hua University, Hsinchu, Taiwan, and National Chiao Tung University, Hsinchu, Taiwan

Received: May 10, 2010; Revised Manuscript Received: August 12, 2010

This work demonstrates a quantitative interpretation of ion desorption in matrix-assisted laser desorption/ionization (MALDI). The theoretical modeling incorporates transition state theory for the desorption of surface ions, assuming chemical and thermal equilibrium in the solid state prior to desorption. It is distinct from conventional models that assume chemical equilibrium in the gas phase. This solid-state thermodynamic interpretation was used to examine the desorption of pure 2,4,6-trihydroxyacetophenone (THAP) and of angiotensin I mixed with THAP. It successfully described the changes in ion yield with the effective temperature under various laser fluence and initial temperature conditions. The analysis also revealed the key role played by ion concentration in the modeling to provide the best fit of the model to observations. On the other hand, divergence of the ion beam with laser fluence was examined using an imaging detection method, and the signal saturation normally seen at high fluence was appropriately reduced by ion focusing. Simplified but deceptive theoretical interpretations were obtained when the analysis was conducted without adequate calibration of the instrument bias.

Introduction

Matrix-assisted laser desorption/ionization (MALDI) is one of the most established techniques for mass analyses,[1−6] but extension of its application is difficult due to the shortage of a reliable reaction model. For instance, it is inefficient for ionizing carbohydrates, although good ion yields are available for proteins and peptides. Other disadvantages of MALDI range from sample handling to data analysis, such as: the sample preparation is a highly empirical process,[4,7,8] the quantification analysis using mass spectra is difficult,[4,9] and the signal reproducibility is poor.[4,7,10] These problems persist mainly because the fundamental ion generating mechanism in MALDI is still not fully understood.

Several reaction models have been proposed in the literature to explain the underlying mechanism. For example, Karas and co-workers proposed in their cluster ionization (CI) model that ions are preformed in crystals as ion pairs,[11,12] and the detected ions are those that survived in unbalanced charge defects or local volumes of crystals. This model was effective for explaining the resultant species qualitatively, but a quantitative interpretation was not developed. Many other models use the concept of laser-induced matrix ionizations, such as the production of matrix ions via multiphoton absorption and the charge redistribution among matrices and analytes in the gas phase. Some examples include the photochemical ionization model proposed by Ehring and co-workers,[13] the thermal ionization model by Allwood and Dyer,[14,15] and the quantitative two-step model by Knochenmuss.[16,17] However, most of these reaction models emphasize the ionization reactions in the gas phase and oversimplify the descriptions of desorption processes.

In contrast to the models focused on ionization, material desorption in MALDI has also been studied experimentally[7,18−21] and theoretically.[22−25] The most important model is the quasi-thermal desorption model[26] proposed by Dreisewerd and co-workers that describes the thermal characteristics, including the influence of sample temperature on ion yield. Experimental support of the temperature effect of this model was also published by the same research group,[27] but the impact of the ionization process was simplified in this model. This inevitably made the model deviate from the situation where desorption and ionization should occur simultaneously in MALDI. A common disagreement between observation and modeling was the pronounced deviation with high laser fluence region, in which a saturation of experimental results was typically seen. Unfortunately, there was insufficient information to determine the source of disagreement. To more precisely describe the MALDI phenomenon, incorporating both ionization and desorption in the quantitative model and reducing experimental bias are highly important.

This study combines both processes, desorption and ionization, in a quantitative thermodynamic interpretation of MALDI. The detection bias at high laser fluence was monitored and reduced by ion focusing. The matrix and the analyte used in this work were 2,4,6-trihydroxyacetophenone (THAP) and angiotensin I (ANG), respectively. The experiments were conducted with various laser fluences and initial sample temperatures, and the effective local temperature as a function of laser fluence was estimated using a thermal confinement approximation. On the basis of the transition state theory, a local equilibrium condition for ion desorption was used to interpret

* Corresponding author. Genomics Research Center, Academia Sinica, 128, Academia Road, Section 2, Nankang District, Taipei 115, Taiwan, R. O. C. Tel.: 886-2-27871272. Fax: 886-2-27899931. E-mail: wer@gate.sinica.edu.tw.

[†] Genomics Research Center, Academia Sinica.

[‡] Taiwan International Graduate Program, Academia Sinica.

[§] National Tsing Hua University.

[||] National Chiao Tung University.

10.1021/jp104250g
Published on Web 10/11/2010

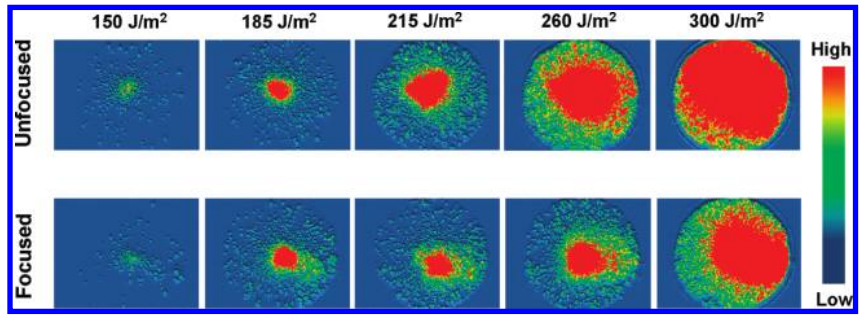

Figure 1. Ion populations detected by imaging MCP with and without ion focusing at various laser fluences. The diameter of the detector area was 40 mm. The palette shows colors denoting the ion intensity in the pictures, and every picture averaged 16 laser shots.

the experimental results. The impact of the coupling of ionization and desorption in the modeling was discussed.

Experimental Section

All experiments were conducted with a laboratory-made time-of-flight (TOF) mass spectrometer equipped with a MALDI source. The instrument was essentially as described previously,[21] except that a new sample electrode, an Einzel lens, and a new detector were installed for this work. The new sample electrode was made of copper in the same dimensions as used earlier, while the stainless steel sample probes to accommodate samples were retained from the previous work. The copper electrode allowed rapid thermalization of the sample for the temperature-dependent measurements. Its temperature was regulated in a range between 120 and 340 K by direct contact with a liquid nitrogen reservoir through an insulating tube and counter-balanced by a quartz halogen lamp near the sample electrode. The temperature was measured by a K-type thermocouple that can be detached from the sample electrode before applying high voltages. The Einzel lens was installed around 1 cm behind the ion source to focus the ion beam.

The new ion detector was a computer-controlled 40 mm imaging MCP detector (Ion Imaging Detector, Photonic Science Ltd., East Sussex, U.K.) able to operate in spectrum mode to record the time-domain signal or imaging mode to monitor the spatial distribution of ions. The electronic circuit to drive the MCP and the phosphor was modified in-house to conduct both modes simultaneously. The images typically averaged 16 laser shots due to limitations of the control software.

Ions were generated by a frequency-tripled Nd:YAG laser beam (355 nm, pulse width ~5 ns, MINILITE I, Continuum, Santa Clara, CA) that examined the sample surface at about 5° from the surface normal. The spot size and beam shape were selected by an iris diaphragm while examining the beam quality using a laser beam profiler (WinCamD-UCM, DataRay Inc., Bella Vista, CA). The laser beam was focused by a fused silica lens ($f = 25$ cm) installed inside the vacuum chamber, resulting in a circular spot size of roughly 250 μm o.d. at the sample surface. The laser fluence was regulated by a circular neutral-density filter. In the initial temperature-dependent experiments, a laser fluence of 210 J/m^2 was typically utilized. Ion intensity was taken as the integration of the corresponding peak area at the molecular weight domain. Every data point in these results was obtained from at least four mass spectra, where every spectrum averaged 100 laser shots.

All chemicals were of analytical grade, and distilled deionized water was used throughout this work. To prepare a pure matrix sample, THAP (Sigma Chemical Co., St. Louis, MO) was dissolved in 50% aqueous acetonitrile (Merck & Co., Inc., Whitehouse Station, NJ) solution to a concentration of 0.1 mmol/mL. The solution was then dropped on the sample target and vacuum-dried to a final amount of 200 nmol on the target. To prepare the mixed sample, ANG (Sigma Chemical Co.) was dissolved in deionized water to a concentration of 0.001 mmol/mL, and then the solution was premixed with the matrix solution in a matrix-to-analyte molar ratio (M/A) of 100. The mixed solution was dropped onto the sample target and vacuum-dried.

Results and Discussion

Divergence of Ion Beam. The ion beam population on the detector increased as the laser fluence increased, as shown in Figure 1. The general shape of the ion beam contained an intense core (red area) and a fuzzy profile (yellow and green). There were also minor ion signals spread out all over the detection area. The population of the unfocused ion beam increased rapidly with increased laser fluence (first row, Figure 1). Below 215 J/m^2, the ion beam projected on the detection area without significant position bias or oversize, but part of the fuzzy profile or the core of the ion beam fell outside the detection area above this fluence. At 300 J/m^2, barely half of the core area was observed. The oversized beam was improved with ion focusing, as can be seen from the slower increase of the ion beam population with increased laser fluence (second row, Figure 1). With focusing, most of the ion beam fell within the detection area below 260 J/m^2, except for minor signals distributed far away from the core area. At a laser fluence of 300 J/m^2, part of the core area and most of the minor signals projected outside the detection area.

The TOF signal intensity agreed with the ion imaging observations, suggesting that divergence of the ion beam was an important factor responsible for the signal saturation seen in the high laser fluence region. The ion intensity obtained with pure THAP was shown in Figure 2, where the appearance threshold of protonated THAP was roughly 150 J/m^2 in this experiment. At fluences below 215 J/m^2, the appearance of ions with (solid circles) and without (open squares) ion focusing was the same; above this fluence, the ion intensity without ion focusing was smaller than that with ion focusing. Such divergence may have originated from increased angular spread and Coulomb repulsion of ions when a greater amount of ions were produced. Although the divergence of ejected neutral particles has been considered by Quist and co-workers,[28] a quantitative correction of ion divergence was still unavailable. Because the beam divergence was not negligible, the rest of the experimental data shown in this work were all obtained with ion focusing.

Establishment of the Quantitative Model. The predicted ion intensity curve was the result of best fitting based on chemical kinetic theory, assuming chemical equilibrium was established for molecules on the surface. It is likely that

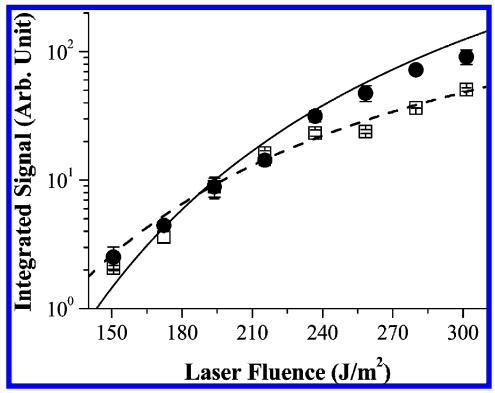

Figure 2. Integrated protonated THAP signal intensity as a function of laser fluence. The solid circles (●) and the open squares (□) represent data obtained with and without postfocusing, respectively. The solid line is the best fitting result including ion concentration. The dashed line is the theoretical prediction without ion concentration.

equilibrium was achieved within the laser-irradiated crystal volume prior to material desorption. Equilibrium was unlikely satisfied in the gas phase because a MALDI plume is a highly dynamic system. On the basis of the solid-state chemical equilibrium concept, the ion signal (I_P) obtained from the spectrum depends on the concentration of surface ions, $[P]_s$, and their desorption rate constant (k_{desorb})

$$I_P \propto k_{desorb}[P]_{(s)} \tag{1}$$

Note that the primary ion in this model refers exclusively to the matrix ion.

It is commonly accepted that the matrix absorbs the laser energy and converts it to thermal energy via internal conversion.[26−28] This implies that MALDI may incorporate thermal-induced chemical processes aside from photoionization, and it is thought that local thermal equilibrium is achieved instantaneously due to fast internal conversion followed by vibrational relaxation.[29−31] However, sharp temperature decreases occurred when material desorption started. Notably, heat dissipation via conduction has generally been neglected in theoretical predictions because it takes time in the order of microseconds or longer,[29] especially for organic solids.[30−32] This suggests that the thermal energy will be confined to the irradiation volume, and the matrix was overheated;[24] the same thermal-confinement approximation was used in this work.

Equation 1 is applicable for most cases even though the primary ions may originate from several possible processes.[33−35] General primary ionization reactions can be expressed as the following chemical reactions promoted by the laser

$$\mathbf{M}_{(s)} + nh\nu \overset{K_1'}{\rightleftharpoons} \mathbf{M}^{\bullet+}_{(s)} + e^- \tag{2}$$

where **M** stands for the matrix and K_1' is the equilibrium constant. The $\mathbf{M}_{(s)}$ denotes a matrix in the solid phase surrounded by the bulk of matrix molecules. Because protonated matrices are normally the final products, the radical cation in eq 2 must react with another neutral matrix molecule to produce the protonated matrix[36]

$$\mathbf{M}_{(s)} + \mathbf{M}^{\bullet+}_{(s)} \overset{K_1''}{\rightleftharpoons} [\mathbf{M} + \mathrm{H}]^+_{(s)} + [\mathbf{M} - \mathrm{H}]^{\bullet}_{(s)} \tag{3}$$

Therefore, the overall reaction combining eqs 2 and 3 becomes

$$2\mathbf{M}_{(s)} + nh\nu \overset{K_1}{\rightleftharpoons} [\mathbf{M} + \mathrm{H}]^+_{(s)} + [\mathbf{M} - \mathrm{H}]^{\bullet}_{(s)} + e^- \tag{4}$$

Equations 2−4 represent a possible reaction sequence that does not directly produce an ion pair, but the matrix radical may react with the electron to produce a negative ion. The protonated matrix may also be produced directly via proton disproportionation

$$2\mathbf{M}_{(s)} + nh\nu \overset{K_1}{\rightleftharpoons} [\mathbf{M} + \mathrm{H}]^+_{(s)} + [\mathbf{M} - \mathrm{H}]^-_{(s)} \tag{5}$$

All the ions are assumed to be in the solid phase upon production. Note that the equilibrium constant (K_1) in the two reaction pathways is assumed to be the same, but different kinds of matrix molecules do not necessarily undergo the same reaction pathway as others.[37] Because the ion-to-neutral ratio reported in the literature was typically in the order of 10^{-5}, this value was used to calculate the K_1 of THAP at its threshold fluence (150 J/m^2 in the present work). On the basis of eqs 2 and 3, the ion concentration ($[P]_s$) in the solid phase was derived and taken into account in our model, in contrast to other works that excluded the ionization from the modeling.[26,27,38] Furthermore, an Arrhenius-form desorption/vaporization rate of the ions can be expressed by the transition state theory[39] as

$$k_{desorb}(T) = \frac{kT}{h}\frac{Q^{\ddagger}(T)}{Q(T)}e^{-\Delta E_a^{\ddagger}/RT} \tag{6}$$

where $\Delta E_a^{\ddagger}$ is the activation energy that is approximately equal to the sublimation enthalpy; T is the temperature; k is the Boltzmann constant; and h is the Planck constant. The $Q^{\ddagger}(T)$ and $Q(T)$ stand for the vibrational partition function of the activated complex and the reactant, respectively. The application of the transition state theory to surface reactions was mentioned previously.[40]

Assuming the temperature change depended linearly on the laser fluence (F), the final temperature can then be expressed as $T = T_0 + \gamma F$, as described by Dreisewerd and co-workers.[26] The γ is the conversion coefficient of laser fluence to surface temperature, which depends on the photochemical properties of the matrix, such as absorption cross section, nonradiative decay rate, and fluorescence quantum yield. Thus, the desorption rate constant as a function of laser fluence becomes

$$k_{desorb}(T) = \frac{k(T_0 + \gamma F)}{h}(1 - e^{-h\nu/k(T_0+\gamma F)})e^{-\Delta E_a^{\ddagger}/R(T_0+\gamma F)} \tag{7}$$

where ν is the vibrational frequency of the intermolecular bond. Combining the $k_{desorb}(T)$ and the ion concentration derived from eq 4 or 5, the yield of protonated THAP (Figure 2) was thus fitted using the formula

$$I_{[M+H]^+} = A\frac{kT}{h}(1 - e^{-h\nu/kT})e^{-\Delta E_{a,[M+H]^+}/RT}\left(\frac{\sqrt{K_1}}{1 + 2\sqrt{K_1}}\right) \tag{8}$$

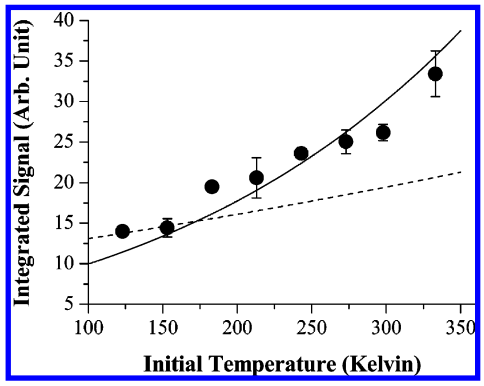

Figure 3. Integrated protonated THAP signal as a function of initial sample temperature. The experimental data were obtained using a fixed laser fluence of 210 J/m^2. The solid line is the result of best fitting including ion concentration. The dashed line is the prediction without ion concentration.

where A was merely a scaling pre-exponential factor in the simulation. When a laser irradiates the sample surface, the temperature burst leads to sublimation of the sample. Because the sublimation enthalpy of THAP was not experimentally available, the predicted value of 100.68 kJ/mol was used based on a quantitative structure property relationship (QSPR) model established by Gharagheizi.[41] The QSPR model was able to predict the sublimation enthalpy of DHB within 2% from the experimental data.[42] The predicted value was used for the $\Delta E_{a,[M+H]^+}$ in eq 8 because the majority of desorbed material was neutral THAP; the ionic THAP was entrained by the neutral THAP during desorption, although the ions may have exhibited higher sublimation enthalpy due to charge−dipole interactions. For protonated THAP, $\nu = 350$ cm^{-1} was used for curve fitting of the observation made with ion focusing. This frequency is a typical value for noncovalent bonds between organic molecules. Adjusting the value from 350 to 1000 cm^{-1} did not produce a significant change to the fitting curves.

Notably, the ion concentration was found to have a significant impact on the modeling. Removing the ion concentration from eqs 1 and 8 (the last term in the equations) produced a curve that was obviously below the observation made with ion focusing (Figure 2). However, the curve excluding the ion concentration agreed with the data obtained without ion focusing, suggesting that a misinterpretation may occur if both instrumental and theoretical biases were not properly calibrated.

Examination of the Reaction Model with Various Temperatures. To examine the impact of initial temperature on the quantitative model, the same measurements were conducted while changing the initial sample temperatures from 120 to 340 K (Figure 3). In this experiment, the laser fluence was fixed at 210 J/m^2 so that enough ions were produced with the lowest sample temperature. The protonated THAP signal decreased evenly with the decrease of initial temperature T_0, and the theoretical prediction agreed well with observation. The best-fit curve without ion concentration (dashed line) showed a remarkable deviation from the observation when above 150 K.

The first-order relationship between the effective local temperature and the laser fluence provided good results in the fitting. Quadratic and cubic fluence dependences had marginal effects on the fitting, which was consistent with the previous reports[14−16] suggesting the important contribution of internal conversion. With pure THAP, $\gamma = 10.9$ Km^2/J was obtained in this work assuming it was a constant in the entire laser fluence range. The presence of impurities, including analytes, may also alter the effective temperature due to their distinct photochemical properties, concentrations, and the rate of energy exchange between the impurities and the matrix.

Application of the Quantitative Model to a Two-Component System. The solid-state thermodynamic interpretation was further challenged using the ANG/THAP two-component system. The protonated ANG was produced by a proton-transfer reaction in the condensed phase, assuming a local equilibrium was achieved

$$[\mathrm{THAP} + \mathrm{H}]^+_{(s)} + \mathrm{ANG}_{(s)} \overset{K_2}{\rightleftharpoons} \mathrm{THAP}_{(s)} + [\mathrm{ANG} + \mathrm{H}]^+_{(s)} \quad (9)$$

where K_2 is the equilibrium constant. This reaction is an analogue of the secondary reaction described in the literature[16,17] except that it was proposed to occur in the condensed phase in this work. Assuming a primary reaction of eq 5, the intensity of the protonated matrix and ANG could be derived from eq 8 with minor modifications

$$I_{[\mathrm{M}+\mathrm{H}]^+} = A'\frac{kT}{h}(1 - e^{-h\nu_{[\mathrm{M}+\mathrm{H}]^+/kT})\cdot e^{-\Delta E_{a,[\mathrm{M}+\mathrm{H}]^+/kT}\cdot} \left(\sqrt{K_1 + zK_1K_2} - \frac{zK_1K_2}{\sqrt{K_1 + zK_1K_2}}\right) \quad (10)$$

$$I_{[\mathrm{ANG}+\mathrm{H}]^+} = A''\frac{kT}{h}(1 - e^{-h\nu_{[\mathrm{ANG}+\mathrm{H}]^+/kT})\cdot e^{-\Delta E_{a,[\mathrm{ANG}+\mathrm{H}]^+/kT}\cdot}\frac{zK_1K_2}{\sqrt{K_1 + zK_1K_2}} \quad (11)$$

where A' and A'' are pre-exponential factors; K_2 is the equilibrium constant of the proton transfer reaction; and z is the analyte-to-matrix ratio ($z = 10^{-2}$ in the present work) in the solid phase. The K_2 was determined experimentally from the intensity of protonated ANG and THAP in the mass spectra. The concentrations of neutral THAP and ANG were assumed to be constants because ion yields are typically below 10^{-5}.

The sublimation enthalpy and the intermolecular vibrational frequency of eq 11 were adopted from those of pure THAP, although the sublimation enthalpy of pure ANG should be much higher and its intermolecular bond frequency should be changed. This assumption is reasonable since ANG coexpanded with a large excess of THAP as the critical sublimation condition of THAP was satisfied.

By changing the laser fluence, a clear protonated THAP signal was observed above 230 J/m^2 (Figure 4), and the maximum fluence used was extended to 380 J/m^2 to allow sufficient data points for theoretical analysis. For protonated THAP, the theoretical prediction agreed reasonably with the experimental result within 400 J/m^2 (Figure 4). The γ value was 9.3 Km^2/J for the best fitting curve, so the effective local temperature was lower than that of pure THAP at the same laser fluence due to the change of thermodynamic property of the crystal. This was also supported by the higher appearance threshold of protonated THAP than the one-component system. The 15% reduction of γ in the ANG/THAP system compared to pure THAP originated from (a) the low extinction coefficient of ANG at the excitation wavelength (<1.4% of that of THAP according to UV spectroscopy) and (b) the increase of average molar heat capacity by the adduction of ANG. Although only 1% of ANG presented in the cocrystal, its contribution was important because the

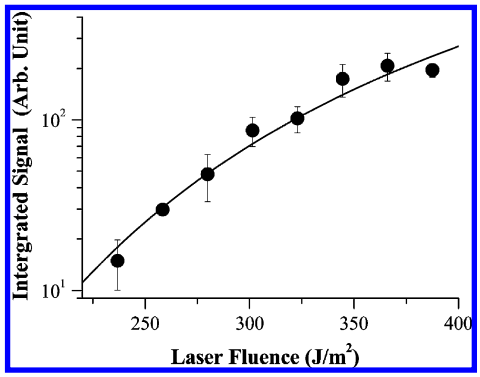

Figure 4. Integrated protonated THAP signal as a function of laser fluence in a two-component system. The solid line is the result of best fitting by the quantitative model.

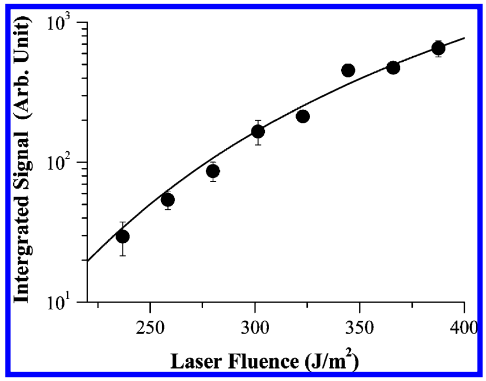

Figure 5. Integrated protonated ANG signal as a function of laser fluence in a two-component system. The solid line is the result of best fitting by the quantitative model.

number of vibrational degrees-of-freedom of ANG is an order of magnitude higher than THAP. This resulted in the reduction of the volume occupancy of THAP by ~7.2% and the increase of the average molar heat capacity by ~8.9%.

Notably, the steep power−law dependence of the protonated ANG on the laser fluence implied the thermodynamic nature of MALDI, which has a value of 7−9 in the literature[43] and 7.6 in the present work (Figure 5). Such steep power−law dependences can not be attributed solely to the multiphoton ionization process of matrix because otherwise the ionization should be very inefficient. In addition, ANG competed for protons and suppressed the protonated THAP, especially when limited amounts of proton were produced under low laser fluences. For a given γ, the reaction Gibbs energy of eq 9 reduced from roughly −109.4 to −187.6 kJ/mol when increasing the laser fluence from 236 to 388 J/m^2. The observation across the same fluence range showed a three-time enhancement of the relative intensity of protonated ANG with respect to protonated THAP. This result indicated that the production of protonated ANG was favorable toward high laser fluence range.

Conclusion

For THAP, the solid-state thermodynamic interpretation described the ion desorption quantitatively, assuming ionization had occurred and chemical and thermal equilibrium were achieved in the condensed phase. Due to the temperature burst, the surface ions desorbed into the gas phase as THAP started to sublimate. The essential distinction of the current interpretation from conventional gas-phase models is the establishment of a virtual-equilibrium in the solid phase, in contrast to the pseudoequilibrium presumption within the highly dynamic plume. Because the equilibrium conditions were logically defined in the solid phase, transition state theory was utilized for the quantitative analysis to replace the arbitrary fitting prefactors generally used. This interpretation described our observations of the pure THAP and the ANG/THAP systems rather well. A higher laser fluence was necessary for ion ejection when analytes with lower optical absorbance and higher heat capacity were used. The beam divergence was found to change the detected ion intensity significantly in the high laser fluence range. Misinterpretation may occur when instrumental biases and imperfect models are involved. Appropriate ion focusing restored the signal intensity, and the observed result was then an adequate match with our prediction. Further study of the sample temperature and thermal-induced chemical reactions of other sample conditions is necessary for the establishment of a reliable interpretation of MALDI. A comprehensive model of the detailed ionization mechanism will be discussed in the future.

Acknowledgment. This work was supported by the Genomics Research Center, Academia Sinica, and the National Science Council of Taiwan (Contract no. NSC 98-2113-M-001-021-MY3).

References and Notes

(1) Karas, M.; Bachmann, D.; Bahr, U.; Hillenkamp, F. *Int. J. Mass Spectrom. Ion Process.* **1987**, *78*, 53–68.
(2) Lee, S.; Winnik, M. A.; Whittal, R. M.; Li, L. *Macromlecules* **1996**, *29*, 3060–3072.
(3) Edwards, J. L.; Kennedy, R. T. *Anal. Chem.* **2005**, *77*, 2201–2209.
(4) Hillenkamp, F.; Peter-Katalinic, J. *MALDI MS: A Practical Guide to Instrumentation, Methods and Applications*; Wiley-VCH: Weinheim, 2007.
(5) Chen, C. H. *Anal. Chim. Acta* **2008**, *624*, 16–36.
(6) Beavis, R. C.; Chait, B. T. *Anal. Chem.* **1990**, *62*, 1836–1840.
(7) Dreisewerd, K. *Chem. Rev.* **2003**, *103*, 395–425.
(8) Horneffer, V.; Gluckmann, M.; Kruger, B.; Karas, M.; Strupat, K.; Hillenkamp, F. *Int. J. Mass Spectrom.* **2006**, *249*, 426–432.
(9) Nelson, R. W.; Mclean, M. A.; Hutchens, T. W. *Anal. Chem.* **1994**, *66*, 1408–1415.
(10) Garden, R. W.; Sweedler, J. V. *Anal. Chem.* **2000**, *72*, 30–36.
(11) Karas, M.; Gluckmann, M.; Schafer, J. *J. Mass Spectrom.* **2000**, *35*, 1–12.
(12) Karas, M.; Kruger, R. *Chem. Rev.* **2003**, *103*, 427–439.
(13) Ehring, H.; Karas, M.; Hillenkamp, F. *Org. Mass Spectrom.* **1992**, *27*, 472–480.
(14) Allwood, D. A.; Dyer, P. E.; Dreyfus, R. W. *Rapid Commun. Mass Spectrom.* **1997**, *11*, 499–503.
(15) Allwood, D. A.; Dyer, P. E.; Dreyfus, R. W.; Perera, I. K. *Appl. Surf. Sci.* **1997**, *110*, 616–620.
(16) Knochenmuss, R. *J. Mass Spectrom.* **2002**, *37*, 867–877.
(17) Knochenmuss, R. *Analyst* **2006**, *131*, 966–986.
(18) Spengler, B.; Bahr, U.; Karas, M.; Hillenkamp, F. *Anal. Instrum.* **1988**, *17*, 173–193.
(19) Puretzky, A. A.; Geohegan, D. B. *Appl. Surf. Sci.* **1998**, *129*, 248–254.
(20) Puretzky, A. A.; Geohegan, D. B.; Hurst, G. B.; Buchanan, M. V.; Luk'yanchuk, B. S. *Phys. Rev. Lett.* **1999**, *83*, 444–447.
(21) Tsai, S.-T.; Chen, C.-H.; Lee, Y. T.; Wang, Y.-S. *Mol. Phys.* **2008**, *106*, 239–247.
(22) Vertes, A.; Irinyi, G.; Gijbels, R. *Anal. Chem.* **1993**, *65*, 2389–2393.
(23) Johnson, R. E. *Int. J. Mass Spectrom. Ion Process.* **1994**, *139*, 25–38.
(24) Zhigilei, L. V.; Garrison, B. J. *J. Appl. Phys.* **2000**, *88*, 1281–1298.
(25) Zhigilei, L. V.; Leveugle, E.; Garrison, B. J.; Yingling, Y. G.; Zeifman, M. I. *Chem. Rev.* **2003**, *103*, 321–347.
(26) Dreisewerd, K.; Schurenberg, M.; Karas, M.; Hillenkamp, F. *Int. J. Mass Spectrom. Ion Process.* **1995**, *141*, 127–148.
(27) Schurenberg, M.; Dreisewerd, K.; Kamanabrou, S.; Hillenkamp, F. *Int. J. Mass Spectrom.* **1998**, *172*, 89–94.
(28) Quist, A. P.; Huthfehre, T.; Sundqvist, B. U. R. *Rapid Commun. Mass Spectrom.* **1994**, *8*, 149–154.
(29) Koubenakis, A.; Frankevich, V.; Zhang, J.; Zenobi, R. *J. Phys. Chem. A* **2004**, *108*, 2405–2410.
(30) Carslaw, H. S.; Jaeger, J. C. *Conduction of Heat in Solids*; Clarendon Press: Oxford Eng., 1947.

(31) Mcdonald, F. A.; Wetsel, G. C. *J. Appl. Phys.* **1978**, *49*, 2313–2322.
(32) Tom, R.; Moore, T. A.; Lin, S. H. *Chem. Phys. Lett.* **1979**, *66*, 390–394.
(33) Liao, P. C.; Allison, J. *J. Mass Spectrom.* **1995**, *30*, 408–423.
(34) Bourcier, S.; Bouchonnet, S.; Hoppilliard, Y. *Int. J. Mass Spectrom.* **2001**, *210/211*, 59–69.
(35) Liu, B.-H.; Lee, Y. T.; Wang, Y.-S. *J. Am. Soc. Mass Spectrom.* **2009**, *20*, 1078–1086.
(36) Zenobi, R.; Knochenmuss, R. *Mass Spectrom. Rev.* **1998**, *17*, 337–366.
(37) Liu, B.-H.; Charkin, O. P.; Klemenko, N.; Chen, C.-W.; Wang, Y.-S. *J. Phys. Chem. B* **2010**, *114*, 10853–10859.
(38) Kinsel, G. R.; Yao, D. Q.; Yassin, F. H.; Marynick, D. S. *Eur. J. Mass Spectrom.* **2006**, *12*, 359–367.
(39) Eyring, H.; Lin, S. H.; Lin, S. M. *Basic Chemical Kinetics*; Wiley: New York, 1980.
(40) Houston, P. L. *Chemical Kinetics and Reaction Dynamics*, 1st ed.; McGraw-Hill: Dubuque, IA, 2001.
(41) Gharagheizi, F. *Thermochim. Acta* **2008**, *469*, 8–11.
(42) Price, D. M.; Bashir, S.; Derrick, P. R. *Thermochim. Acta* **1999**, *327*, 167–171.
(43) Westmacott, G.; Ens, W.; Hillenkamp, F.; Dreisewerd, K.; Schurenberg, M. *Int. J. Mass Spectrom.* **2002**, *221*, 67–81.

JP104250G